ALITHEA GENOMICS

WHITE PAPER

MERCURIUS™ 1536 DRUG-seq Generates Reproducible Ultra-High-Throughput Transcriptomic Perturbation Datasets That Decipher Compound Mechanisms of Action and Toxicity Pathway Activation

Alexandre Coudray[1], Elodie Koenig[1], Maya Wilson[2], Elizabeth Bourne[2], Mark Ofield[2], Yaoyao Xiong[2], Greg Slodkowicz[2], Adam Peall[2], Alix Buu Hoang[1], Vincent Hahaut[1], and Daniel Alpern[1]

[1] Alithea Genomics, Epalinges, Switzerland
[2] Arctoris, Abingdon, United Kingdom

Key Takeaways

Screening-scale transcriptomics with over 12,000 genes detected per sample from just 800 plated HepG2 cells at a sequencing depth of 0.7 million reads per sample.

High reproducibility across two independently processed 1536-well plates, with highly correlated inter-plate differentially expressed (DE) gene counts ($R^2 = 0.94$).

Unsupervised transcriptional clustering correctly grouped compounds by known mechanism of action (MoA), including PPARγ agonists, proteasome inhibitors, ER stress inducers, and topoisomerase inhibitors.

Concordant transcriptomic points of departure (tPODs) and dose-response profiles were observed across both independently processed replicate plates.

Compound-specific activation of 18 toxicity-associated pathways and 14 MoA signatures was detected, including DNA damage, ER stress, ferroptosis, and apoptosis, consistent with known biology.

Gene-level resolution distinguished known topoisomerase II inhibitors by potency and revealed a compound-specific ferroptosis signature in mitoxantrone associated with repression of *GPX4* and *SLC7A11*.

Transcriptomic apoptosis signatures were detected at lower doses than measurable cytotoxicity on the same plate, demonstrating earlier compound-stress detection than viability endpoints alone.

Automated 1536-well plate preparation using precision liquid handling systems facilitates high-quality cell and compound dispensing for intra/inter-plate reproducibility, as well as parallel readouts that add a rich layer of information to transcriptomic data.

Prefer a webinar? Watch the presentation of this data in our MERCURIUS™ 1536 DRUG-seq launch webinar.

Introduction

Despite rapidly growing investment in AI-enabled drug discovery and development, biopharma remains constrained by a lack of technologies capable of generating biologically informative, standardized, high-resolution perturbation datasets at the scale required to train predictive models that help reduce pipeline attrition (1).

High-throughput screening (HTS) teams and AI-enabled drug discovery programs have adopted scalable Cell Painting in 1536-well plates for AI model training, but the technology primarily captures downstream morphological phenotypes rather than direct measurements of early transcriptional pathway responses (2–4). Transcriptomic profiling adds a complementary molecular data layer for AI models, which helps to improve their ability to identify compound mechanisms of action (MoA), detect toxicity pathway activation, and estimate safe transcriptomic points of departure (tPODs) (3,4).

However, until now, scalable transcriptomics has required trade-offs between biological resolution and throughput (5). Probe-based approaches, such as L1000, measure only a subset of genes, whereas transcriptome-wide methods, such as single-cell RNA-seq and its variations, have struggled to scale beyond 96-well formats to the 1536-well plates required for large compound perturbation and dose-response datasets that are AI-ready (6–8).

Here, we introduce MERCURIUS™ 1536 DRUG-seq, an ultra-high-throughput, RNA-extraction-free, 3′ mRNA-seq data-generation technology purpose-built for biopharma to produce datasets containing hundreds of thousands to millions of perturbation profiles with the scale, standardization, reproducibility, and biological resolution required for AI model training.

To demonstrate the potential scalability and inter-plate reproducibility of MERCURIUS™ 1536 DRUG-seq, we used automated experimental execution enabled by Arctoris' Ulysses® platform. Ulysses® was used to automate key experimental steps, including compound plate preparation, cell dispensing, viability assessment and downstream processing, enabling reproducible 1536-well scalability for MERCURIUS™ DRUG-seq. Using this integrated workflow, we performed a perturbation screen using 33 compounds with known mechanisms of action (MoA). With 2.5 nL resolution, a custom range of eight doses was designed for each compound, including five technical replicates for a total of 264 conditions per plate. We generated two identical but independently processed 1536-well plates, with only 800 HepG2 cells per well.

We show that MERCURIUS™ 1536 DRUG-seq generates highly reproducible, transcriptome-wide perturbation-response datasets across independently processed 1536-well plates and provides the consistency and biological resolution needed to distinguish compound MoAs and detect toxicity pathway activation without prior pathway annotation, while establishing robust tPODs and dose-response curves. At the gene level, we demonstrate that the technology resolves mechanistic differences among compounds sharing the same MoA, revealing compound-specific pathway signatures that are inaccessible to 'standalone' probe-based or morphological profiling methods. We also show how pairing the technology with a conventional 1536-well cell viability assay on the same plate enables users to detect transcriptomic apoptosis pathway activation that precedes measurable cytotoxicity.

Looking ahead, this in-plate multiplexing can be expanded with high-content imaging readouts like Cell Painting, providing rich morphological insights alongside transcriptomic data, all from a single well.

Methods

Experimental Design, Automation, and Compound Dosage

To assess the reproducibility of MERCURIUS™ 1536 DRUG-seq across independent replicate plates receiving the exact same compound treatments and dosages, Arctoris leveraged its proprietary Ulysses® platform to develop an automated workflow using precision liquid handling to plate 800 HepG2 cells per well across two MERCURIUS™ 1536 DRUG-seq plates (Plate 1 and Plate 2). A curated set of 33 compounds with known MoAs was pre-prepared in assay-ready 1536-well plates using the Beckman Coulter Echo Access Workstation and frozen at –20 °C. On the day of seeding, cells were dispensed on top using the Agilent BioTek MultiFlo FX. Plates were briefly centrifuged at 200 × g for 1 minute before incubation at 37 °C for 24-hour treatments.

Each compound was prepared in an eight-point dose-response with five replicates per condition per plate, with DMSO normalization across all wells. As activity ranges differ by compound, we included a total of 49 unique doses, from low concentrations such as 9.95×10^{-6} to 0.02985 µM for bortezomib to higher concentrations such as 0.0149 to 49.75 µM for pioglitazone (Fig. 1). These doses were chosen based on IC50 values for each compound. To avoid edge effects, the outer edge of each plate was excluded from compound treatment. Compounds and 60 DMSO-treated controls were placed in random wells across each plate to avoid positional effects in downstream differential expression (DE) analysis.

Following compound treatment, CellTiter-Blue® (CTBlue) viability reagent was added to the plates using the SPT Dragonfly. Plates were incubated at 37 °C for 1 hour before reading on a BMG ClarioSTAR to assess condition viability against DMSO-only controls. Cells were then gently washed with PBS to remove the CTBlue reagent using the Agilent Bravo. Finally, all PBS was removed and plates were stored dry at –80 °C.

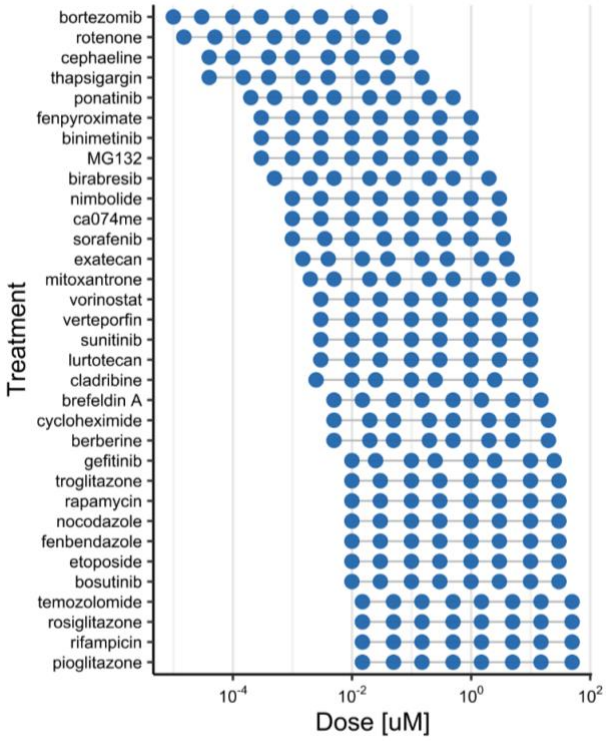

Figure 1. MERCURIUS™ 1536 DRUG-seq experimental design for compound perturbation profiling at scale. *Dose ranges for each of the 33 compounds across eight dose ranks. The broad dose range was selected to capture sub-threshold, threshold, and saturating responses across compounds with diverse potencies and MoAs.*

Library Preparation, Sequencing, and Bioinformatics

The overall plate handling and subsequent RNA-extraction-free library preparation workflow, in which 1536 samples are uniquely 3' barcoded, reverse transcribed, and pooled into a single tube, was performed as described in the user guide and in our accompanying MERCURIUS™ 1536 DRUG-seq technical note.

Additionally, to enable independent, orthogonal quality control of RNA recovery and cell viability across all samples, ERCC RNA Spike-In Mix was added at a fixed concentration to each sample prior to library preparation (9).

Libraries were sequenced with AVITI™ to a depth between 0.6 and 0.8 million reads per sample,

followed by mapping with STAR. DE analysis was performed with DESeq2 (10) per condition relative to DMSO controls (fold change > 1.5, FDR < 0.05). Uniform Manifold Approximation and Projection (UMAP) plots were generated with standard parameters. Toxicity mechanism scores were calculated based on the MAYA method (11) and represent normalized pathway-level activity (0–1 scale) derived from curated gene sets associated with each toxicity category.

Results

MERCURIUS™ 1536 DRUG-seq Detects Over 12,000 Genes Per Sample Reproducibly Across Independent Plates

After processing the plates and sequencing, samples were demultiplexed using their unique well-specific barcodes. More than 96% of reads were successfully demultiplexed and assigned to their correct sample of origin in both plates (Fig. 2A). Between 58% and 60% of these reads uniquely mapped to exons in both instances, indicating reproducible, high-throughput transcriptomic data across replicate plates (Fig. 2B).

We next assessed the sensitivity of gene detection at 0.7 million reads per sample. Despite each well containing only 800 HepG2 cells and being sequenced at ultra-low read depths, both Plate 1 and Plate 2 replicates detected over 12,000 genes (Fig. 2C). The majority of these genes had low (CPM > 0, < 10) to medium (CPM > 10, < 100) expression levels and were consistent across independent plates, indicating the high sensitivity and reproducibility of the assay (Fig. 2D).

To determine whether variation in sequencing depth across the compound library reflected technical inconsistency in library preparation versus true biological differences in input material, we used ERCC spike-in RNAs as an internal control. ERCC spike-ins are a set of synthetic, polyadenylated RNA transcripts of known sequence and quantity that are added to each sample at a fixed concentration prior to library preparation (9). Because they are spiked in at equal amounts regardless of sample content, their recovery serves as a benchmark for technical variability independent of biological differences between samples. We plotted normalized ERCC counts (nERCC) against sequencing depth for all samples across both plates (Fig. 2E). If depth-driven variability were largely technical, ERCC recovery would be expected to track closely with depth. Instead, the correlation between depth and nERCC was weak in both plates ($R = 0.369$ and $R = 0.212$ for Plate 1 and Plate 2, respectively), indicating that ERCC abundance varied largely independently of sequencing depth. This suggests that the observed differences in depth are not primarily an artifact of well-to-well library preparation variability, but instead reflect genuine biological differences between samples, such as cell number, viability, and transcriptional activity, which scale sequencing depth together with endogenous (non-spike-in) content.

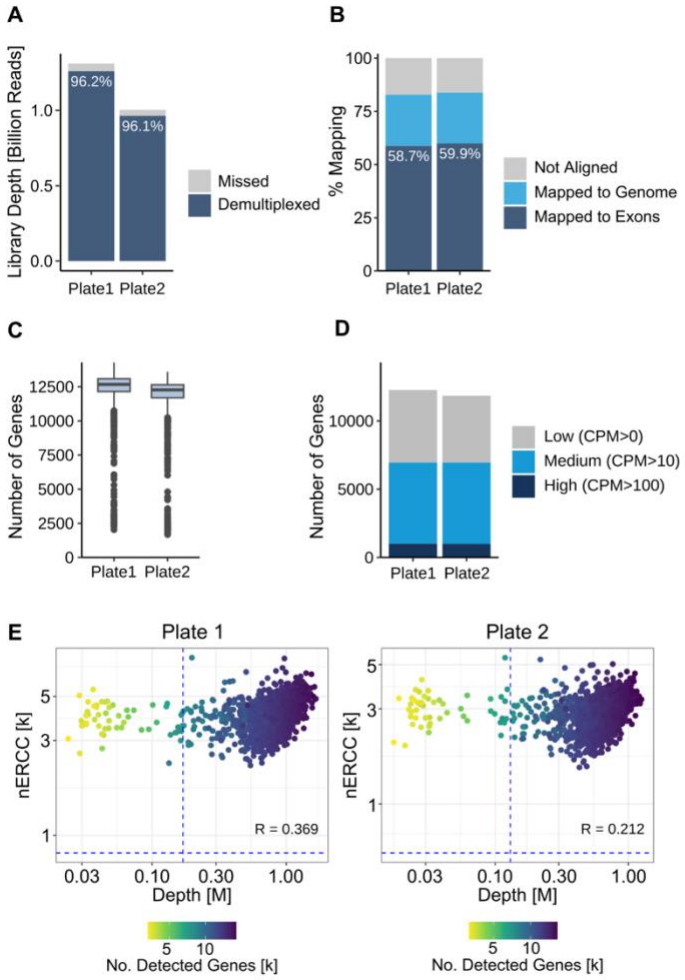

Figure 2. MERCURIUS™ 1536 DRUG-seq quality control metrics and gene detection rates across two replicate plates. *(A) Demultiplexing rates for Plate 1 and Plate 2, demonstrating robust and reproducible sample assignment exceeding 96%. (B) Mapping statistics indicating the proportion of reads mapping to exons, the broader genome, or unaligned. (C) Gene detection rates for both plates, showing median detection of over 12,000 genes per sample at an average depth of 0.7M reads per sample. (D) Stacked bar plot showing the number of genes detected at different expression thresholds. (E) Scatter plots showing the relationship between sequencing depth and normalized ERCC spike-in read counts (nERCC) for all samples in Plate 1 and Plate 2, colored by number of detected genes. The low correlation between depth and nERCC indicates that variation in ERCC abundance is predominantly driven by biological differences among samples rather than technical variation. Dashed lines show QC cutoffs of 20% of median depth (vertical) and 20% of median ERCC counts (horizontal).*

Batch-Corrected Transcriptional Profiles Resolve Compound- and Dose-Dependent Biological Structure

Next, to assess the effect of batch correction, read depth per sample, compound treatment, and dosage on sample clustering, we combined Plate 1 and Plate 2 data using batch correction, followed by unsupervised UMAP clustering. Plate 1 and Plate 2 samples exhibited comparable clustering patterns, supporting the effectiveness of batch correction (Fig. 3A). Several clusters displayed lower read depths compared with the majority of non-clustered samples (Fig. 3B), and these clusters were enriched for specific compounds (Fig. 3C) and doses (Fig. 3D), suggesting that reduced read depth may reflect treatment-associated effects rather than technical variation alone.

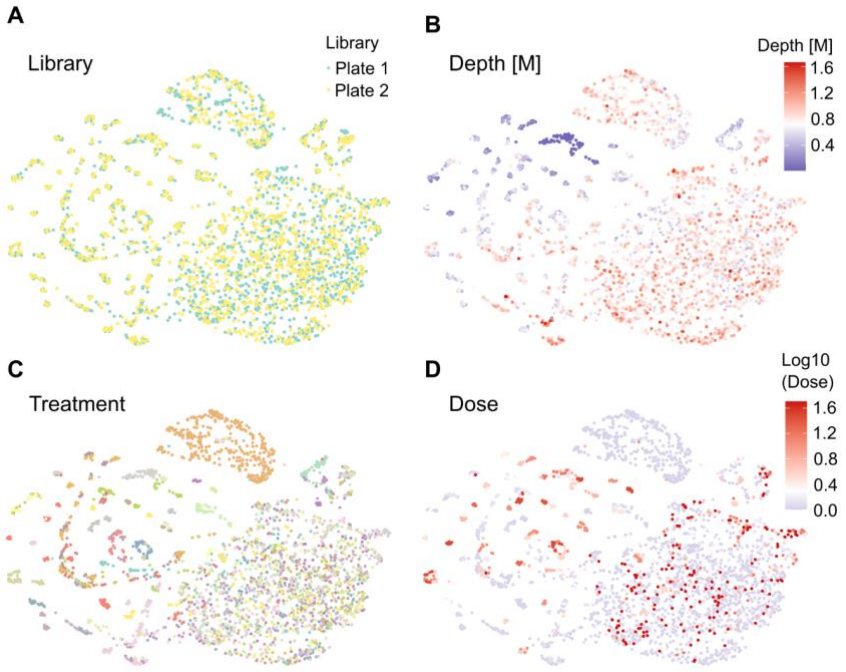

Figure 3. UMAP visualization of 2,760 batch-corrected transcriptional profiles from 33 compounds across eight dose ranks in Plate 1 and Plate 2 replicate plates. *Each point represents a single sample, colored by (A) library, (B) read depth per sample, (C) treatment identity, and (D) dose. Compounds and doses with strong transcriptomic effects largely cluster separately from the central mass of lower-activity treatments, confirming that MERCURIUS™ 1536 DRUG-seq resolves biologically meaningful, compound- and dose-associated transcriptional responses across a diverse perturbation library.*

Unsupervised Clustering Determines Compound MoA and Toxicity Pathway Signatures

To determine transcriptional relationships among compounds in our library grouped by MoA, we next clustered compounds based on their average gene expression profiles using the 5,000 most variable genes to generate a treatment similarity heatmap (Fig. 4A). This analysis revealed strong clustering of PPARγ agonists (troglitazone, pioglitazone, and rosiglitazone), translation inhibitors (cycloheximide and cephaeline), proteasome inhibitors (MG132 and bortezomib), ER stress inducers (thapsigargin and brefeldin A), and topoisomerase inhibitors (mitoxantrone, etoposide, lurtotecan, and exatecan). The latter group also clustered with cladribine, a purine nucleoside analog, consistent with its reported ability to induce DNA lesions.

We next performed pathway activity scoring across a panel of 18 toxicity mechanisms and 14 relevant MoA signatures. For each treatment, we reported the highest pathway score observed across all tested doses (Fig. 4B), revealing marked treatment-specific patterns. For example, thapsigargin and brefeldin A induced a strong endoplasmic reticulum (ER) stress response, whereas topoisomerase inhibitors activated DNA damage signaling together with their corresponding MoA signatures. Interestingly, cycloheximide, a translation inhibitor, also clustered with the topoisomerase inhibitors in this analysis. Rather than reflecting genotoxic stress, this pattern is consistent with a well-described indirect mechanism: because translation inhibitors block synthesis of short-lived proteins, they deplete MDM2, the principal negative regulator of p53, leading to p53 stabilization and activation of downstream p53 target genes in the absence of actual DNA damage (12,13). Since many DNA damage transcriptional signatures are built substantially on p53 pathway targets, cycloheximide's clustering with topoisomerase inhibitors likely reflects convergent activation of p53 signaling through this MDM2-dependent route rather than a shared genotoxic mechanism.

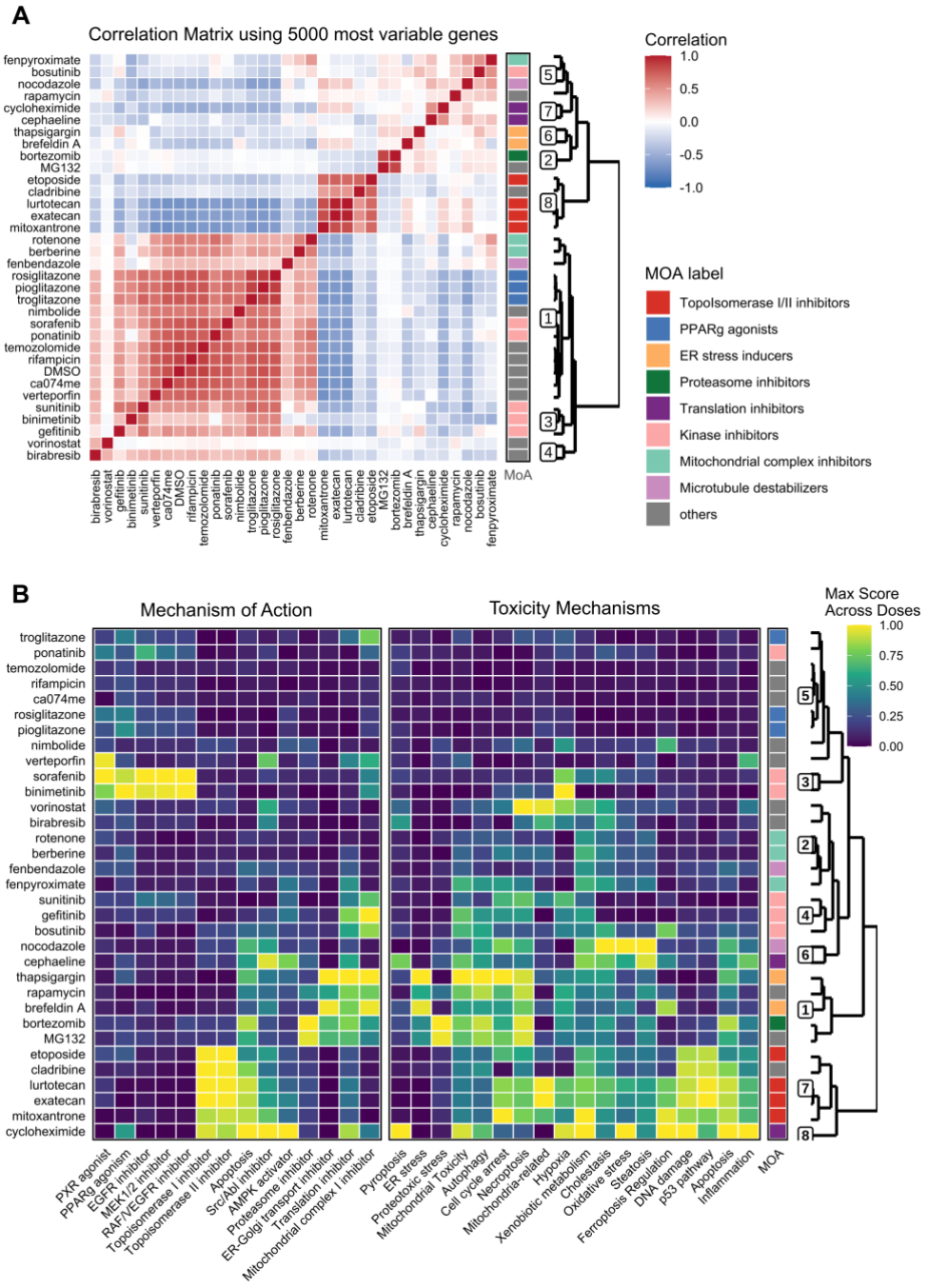

Figure 4. MERCURIUS™ 1536 DRUG-seq resolves compound transcriptional similarity and mechanism-specific pathway activation. *(A) Correlation matrix of average gene expression profiles across the 5,000 most variable genes for all 33 compounds, with compound labels color-coded by MoA class. Compounds with related MoAs form discrete clusters of high transcriptional correlation, including topoisomerase I/II inhibitors, PPARγ agonists, ER stress inducers, proteasome inhibitors, and translation inhibitors. (B) Heatmaps showing the maximum normalized toxicity-related pathway scores (left) and MoA scores (right) across all doses for each compound. Pathway and MoA activation patterns are compound-specific and complementary. Together, MERCURIUS™ 1536 DRUG-seq captures both the shared transcriptional responses of mechanistically related compounds and the distinct pathway signatures that differentiate them.*

Gene-Level Resolution Distinguishes Mechanistically Related Compounds and Uncovers Known Compound-Specific Pathway Signatures

As transcriptomic profiling provides sensitive, gene-level resolution, we next explored the role of particular gene dysregulation in response to distinct topoisomerase II inhibitors. UMAP embedding revealed a clear separation of samples with high DNA damage scores, as indicated by the topoisomerase inhibitors mitoxantrone and etoposide (Fig. 5A). From the whole compound library, six compounds elicited a pronounced DNA damage response, four of which were topoisomerase inhibitors (Fig. 5B). Notably, mitoxantrone and etoposide displayed highly similar transcriptional profiles, reflected in the coordinated regulation of genes associated with topoisomerase II inhibition, consistent with their shared MoA (Fig. 5C).

Despite these transcriptional similarities, comparative gene-level analysis identified notable differences between the two compounds that likely contribute to their separate UMAP clustering. First, mitoxantrone activated its MoA-related signature at substantially lower doses than etoposide, indicating greater potency (Fig. 5C,D), consistent with reports that mitoxantrone is a more potent topoisomerase II poison in cell-based assays, forming more stable cleavable complexes at lower intracellular concentrations than etoposide (14). In addition, mitoxantrone uniquely exhibited a transcriptional signature suggestive of ferroptosis induction, potentially associated with repression of the key ferroptosis regulators GPX4 and SLC7A11 (Fig. 5C,D). GPX4 encodes the glutathione peroxidase that directly detoxifies lipid peroxides, and its loss is sufficient to trigger ferroptosis, while SLC7A11 encodes xCT, which imports the cystine required for glutathione synthesis (15,16). Repression of SLC7A11 limits the glutathione pool available to GPX4; loss of expression of both proteins would be expected to sensitize cells to iron-dependent lipid peroxidation.

Together, these toxicity mechanism data indicate that MERCURIUS™ 1536 DRUG-seq can capture the shared biology of compounds with high accuracy while also resolving their specific differences. For example, among the topoisomerase inhibitors mitoxantrone and etoposide, both induce DNA damage, but only mitoxantrone affects the ferroptosis regulatory pathway, indicating distinct mechanisms that are difficult to identify without transcriptomics.

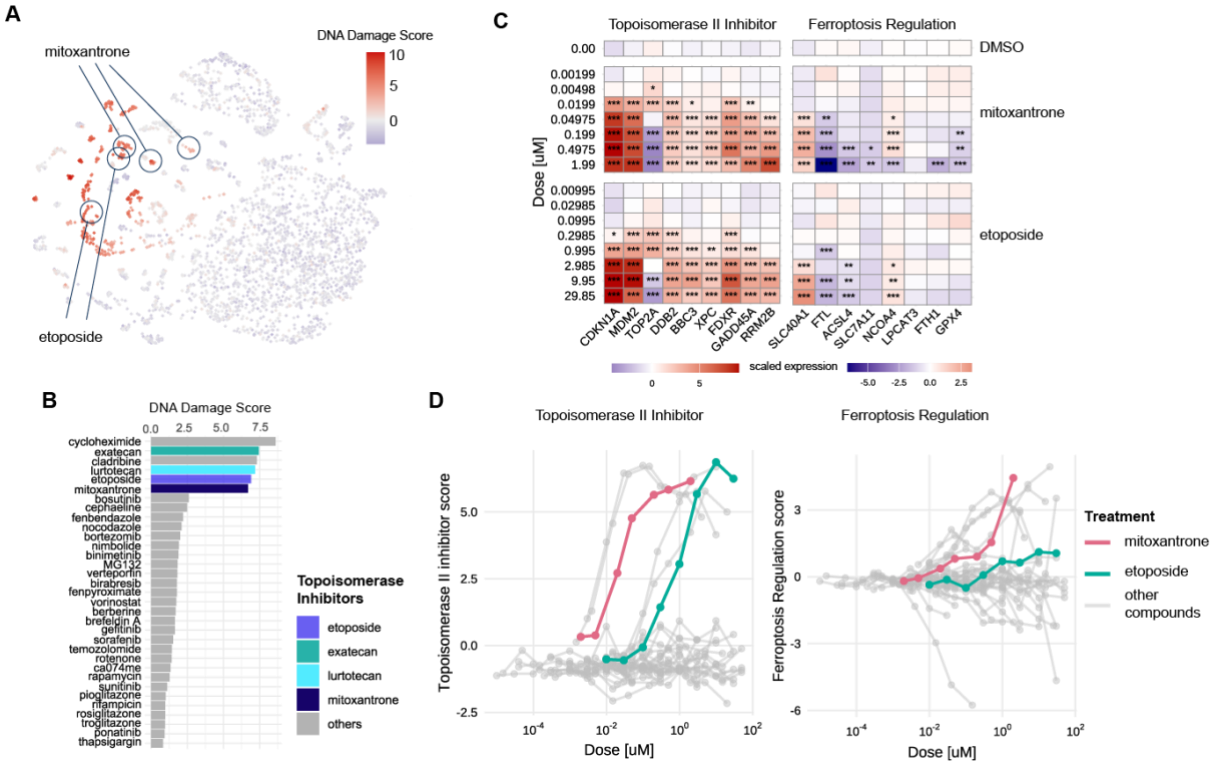

Figure 5. MERCURIUS™ 1536 DRUG-seq distinguishes mechanistically related topoisomerase II inhibitors by potency and identifies a compound-specific, gene-level ferroptosis signature. *(A) UMAP embedding of batch-corrected transcriptional profiles colored by DNA damage score, showing that mitoxantrone and etoposide form discrete high-scoring clusters consistent with their established topoisomerase II inhibitor MoA. (B) Bar chart of maximum DNA damage scores across all doses for all 33 compounds, with topoisomerase inhibitors color-coded by compound. (C) Gene-level scaled expression heatmaps for mitoxantrone and etoposide across all tested doses for genes associated with topoisomerase II inhibition (left) and ferroptosis regulation (right); asterisks indicate statistical significance (* FDR < 0.05, ** FDR < 0.01, *** FDR < 0.001). (D) Dose-response curves for topoisomerase II inhibitor scores (left) and ferroptosis regulation scores (right) for mitoxantrone, etoposide, and all other compounds.*

Transcriptomic Apoptosis Signatures Can Precede Measurable Cytotoxicity in Dose-Response Profiling

As MERCURIUS™ 1536 DRUG-seq is performed in 1536-well plates, it can readily be combined with traditional, high-throughput single-endpoint readouts, such as the CTBlue fluorescence-based cell viability assay, on the same plate. We therefore obtained a simultaneous dual readout of cell viability and transcriptional response to treatment for all 33 compounds tested.

As the topoisomerase II inhibitors mitoxantrone and etoposide share the same MoA but have distinct gene-level transcriptional profiles (Fig. 5C), we next assessed their effects on cell viability, transcriptional activation of the apoptosis pathway, and the proportion of ERCC reads detected, to gain a comprehensive, multimodal understanding of compound effects. ERCC relative abundance serves as an internal standard for mRNA recovery, where an increase in the percentage of ERCC reads reflects a proportional decline in cellular mRNA, providing independent quantitative confirmation of cell death orthogonal to both CTBlue and transcriptomic apoptosis readouts.

For mitoxantrone, cell viability was anti-correlated with transcriptomic apoptosis scores, suggesting that transcriptomics is a reliable proxy for cell viability (Fig. 6). This was also reflected in a higher percentage of ERCC reads at cytotoxic doses, indicating a lower relative abundance of cellular mRNA and increased cell death in these samples (Fig. 6). In contrast, despite sharing the same MoA as mitoxantrone, etoposide showed an increase in apoptosis scores across the dosing range before any major effect on cell viability or the proportion of ERCC reads occurred. This suggests that transcriptomics detects the onset of apoptosis earlier than overt cytotoxicity is detected with single-endpoint assays (Fig. 6).

Together, this example of two compounds with the same overall MoA but distinct effects on other mechanistic pathways, apoptosis, and cellular viability demonstrates the suitability of MERCURIUS™ 1536 DRUG-seq for comprehensive compound profiling at scale, providing earlier insight into compound-specific mechanisms, toxicity-associated pathways, or compromised cell viability than current apical endpoint readouts alone. This higher-resolution characterization of compound-specific stress responses represents the kind of mechanistically interpretable signal that AI models require to learn the transcriptional consequences of cytotoxic compounds.

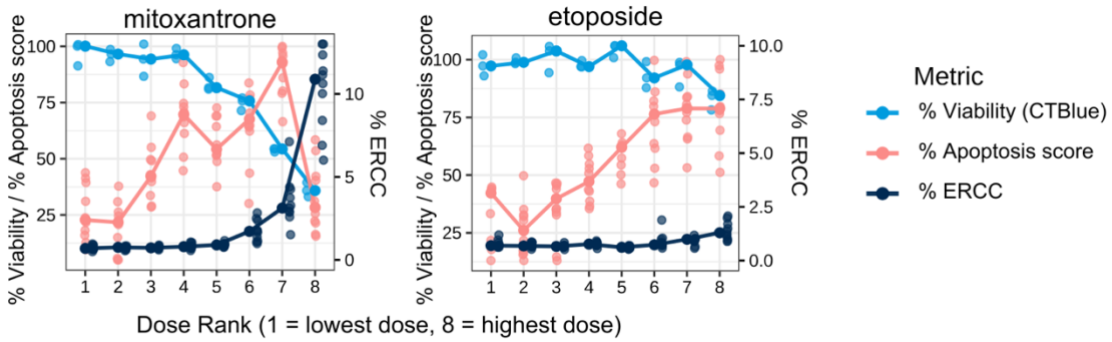

Figure 6. Transcriptional apoptosis signatures align with, and in some cases precede, cytotoxicity in MERCURIUS™ 1536 DRUG-seq dose-response profiling. *Dose-response curves for two topoisomerase II inhibitors showing cell viability determined by the CTBlue cell viability assay (light blue), transcriptomic apoptosis pathway score (red), and ERCC spike-in control recovery (dark blue) across eight dose ranks. For mitoxantrone (left), transcriptomic apoptosis scores anti-correlate with cell viability, confirmed by an orthogonal increase in the percentage of ERCC reads. For etoposide (right), transcriptomic apoptosis signatures increase at lower dose ranks than the corresponding decline in cell viability, with stable ERCC recovery confirming that the observed changes reflect a genuine biological signal rather than a technical artifact.*

Consistent tPODs and Dose-Response Profiles Across Independently Processed Plates Confirm Inter-Plate Reproducibility

Next, as each compound in our library had a particular dose range, we aimed to define tPODs for all compounds. tPODs are the doses that mark the earliest significant changes in gene expression following compound treatment and serve as a protective threshold for regulatory risk assessment, often preceding traditional apical toxicity endpoints (17).

To establish tPODs in our MERCURIUS™ 1536 DRUG-seq data, we performed a DE analysis comparing compound-treated versus DMSO-treated controls for Plate 1 and Plate 2 combined, after batch correction (18). As each compound was tested across a distinct concentration range optimized for its known potency (Fig. 1), tPOD dose ranks reflect the earliest point of transcriptional response within each

compound's own dose range rather than a direct cross-compound potency comparison. Across the compound library, tPODs were largely unimodal, as most compounds showed a clear threshold dose rank below which no significant DE genes were detected and above which DE gene counts increased progressively. This confirms that MERCURIUS™ 1536 DRUG-seq generates structured, interpretable dose-response data suitable for tPOD derivation at screening scale (Fig. 7A).

Next, to assess the reproducibility of MERCURIUS™ 1536 DRUG-seq DE gene detection and dose-response curves across replicate plates, we performed DE analyses independently for Plate 1 and Plate 2. Both plates showed high concordance in DE gene detection across diverse compounds and doses, with tPOD profiles and numbers of DE genes highly correlated between Plate 1 and Plate 2 replicates despite their independent experimental processing (Fig. 7B,C). This highlights the high consistency of both the technical and biological performance of MERCURIUS™ 1536 DRUG-seq across independent plate replicates, using a readout typically applied to evaluate compound activity and potency.

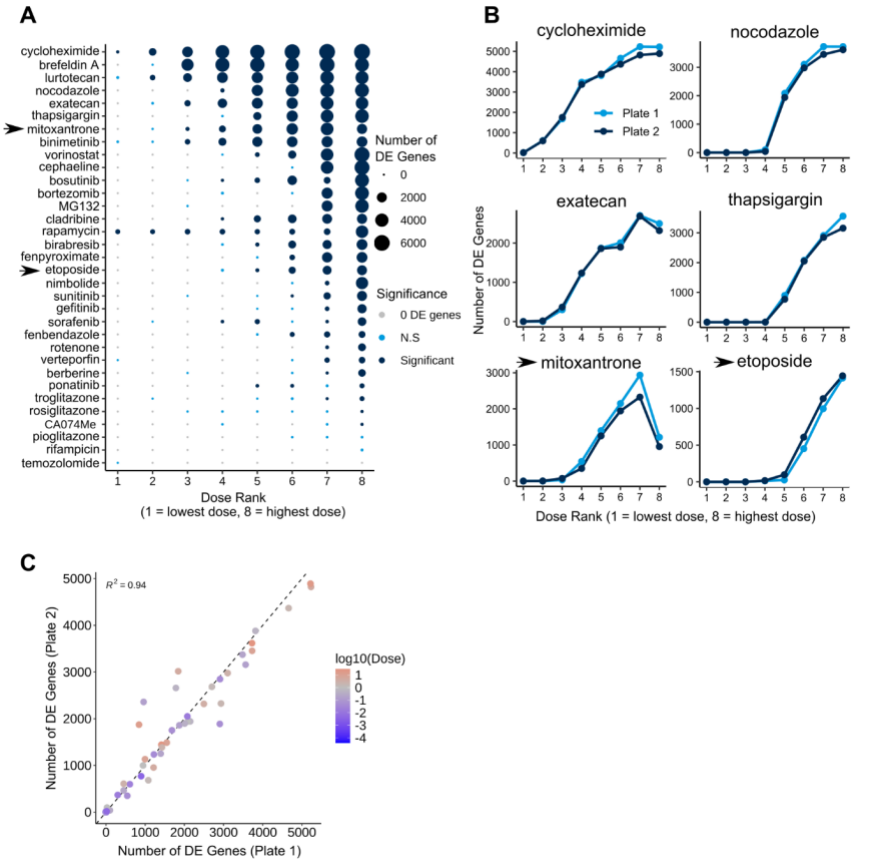

Figure 7. MERCURIUS™ 1536 DRUG-seq detects highly reproducible, dose-dependent transcriptional responses across diverse compounds. *(A) Bubble plot showing the number of DE genes for 33 compounds across eight dose ranks, ordered by the dose rank of the first significant transcriptional response within each compound's individual concentration range. Compounds with diverse MoA exhibit distinct dose-dependent tPODs, ranging from those that elicit strong transcriptional responses at low doses to those that require near-saturating concentrations. (B) Dose-response curves for six representative compounds, showing the number of DE genes across eight dose ranks in Plate 1 and Plate 2. (C) Scatter plot comparing the number of DE genes per compound-dose combination between Plate 1 and Plate 2, colored by log10-transformed dose concentration. The strong correlation between plates (R^2 = 0.94) confirms that MERCURIUS™ 1536 DRUG-seq generates highly reproducible transcriptomic readouts across independently processed 1536-well plates.*

Conclusion

These results demonstrate that MERCURIUS™ 1536 DRUG-seq generates scalable, reproducible, and biologically interpretable ultra-high-throughput transcriptomic data from compound perturbation screens at true screening scale. Across two identical but independently processed 1536-well plates, the technology detected over 12,000 genes per sample from just 800 HepG2 cells at 0.7 million reads per sample, with concordant gene detection and dose-response trajectories across replicate plates. ERCC spike-in recovery confirmed that the variation in sequencing depth observed between samples reflects genuine differences in cellular transcriptional activity and viability rather than technical assay inconsistency, further validating the reliability of the technology for AI model training.

Beyond technical reproducibility, unsupervised clustering of transcriptional profiles correctly grouped compounds by known MoA, including PPARγ agonists, proteasome inhibitors, ER stress inducers, and topoisomerase inhibitors, without prior pathway annotation, demonstrating that MERCURIUS™ 1536 DRUG-seq captures biologically meaningful structure in perturbation data. At the gene level, the technology distinguished between mechanistically related topoisomerase II inhibitors, correctly identifying mitoxantrone as more potent than etoposide and revealing a compound-specific ferroptosis signature in mitoxantrone associated with repression of GPX4 and SLC7A11 — a finding that would be inaccessible to probe-based or morphological profiling methods.

When combined with conventional cell viability assays on the same 1536-well plate, MERCURIUS™ 1536 DRUG-seq detected transcriptomic activation of the apoptosis pathway in etoposide before any corresponding decline in cell viability was measurable by CTBlue, whereas mitoxantrone showed a strong anti-correlation between apoptosis scores and viability, consistent with rapid cytotoxicity. This demonstrates that high-throughput transcriptomics provides a higher-resolution, earlier window into compound-specific stress responses than conventional apical endpoints alone.

Together, these findings establish MERCURIUS™ 1536 DRUG-seq as a core technology for generating the large-scale, standardized, and mechanistically resolved perturbation datasets needed to build proprietary, AI-ready data assets. From unsupervised MoA clustering to gene-level mechanistic differentiation between related compounds, the biological resolution of this data is well suited to train AI models that can predict compound MoA, anticipate toxicity pathway activation, and prioritize candidates with greater confidence earlier in the drug development pipeline.

Questions about implementing MERCURIUS™ 1536 DRUG-seq in your existing screening pipeline? **Reach out to speak to our experts.**

References

1. Zhang K, Yang X, Wang Y, Yu Y, Huang N, Li G, Li X, Wu JC, Yang S. Artificial intelligence in drug development. Nature Medicine. 2025 Jan;31(1):45–59.
2. Fredin Haslum J, Lardeau CH, Karlsson J, Turkki R, Leuchowius KJ, Smith K, Müllers E. Cell Painting-based bioactivity prediction boosts high-throughput screening hit-rates and compound diversity. Nature Communications. 2024 Apr 24;15(1):3470.
3. Haghighi M, Caicedo JC, Cimini BA, Carpenter AE, Singh S. High-dimensional gene expression and morphology profiles of cells across 28,000 genetic and chemical perturbations. Nature Methods. 2022 Dec;19(12):1550–7.
4. Way GP, Natoli T, Adeboye A, Litichevskiy L, Yang A, Lu X, Caicedo JC, Cimini BA, Karhohs K, Logan DJ, Rohban MH. Morphology and gene expression profiling provide complementary information for mapping cell state. Cell Systems. 2022 Nov 16;13(11):911–23.
5. Ye C, Ho DJ, Neri M, Yang C, Kulkarni T, Randhawa R, Henault M, Mostacci N, Farmer P, Renner S, Ihry R. DRUG-seq for miniaturized high-throughput transcriptome profiling in drug discovery. Nature Communications. 2018 Oct 17;9(1):4307.
6. Subramanian A, Narayan R, Corsello SM, Peck DD, Natoli TE, Lu X, Gould J, Davis JF, Tubelli AA, Asiedu JK, Lahr DL. A next generation connectivity map: L1000 platform and the first 1,000,000 profiles. Cell. 2017 Nov 30;171(6):1437–52.
7. Srivatsan SR, McFaline-Figueroa JL, Ramani V, Saunders L, Cao J, Packer J, Pliner HA, Jackson DL, Daza RM, Christiansen L, Zhang F. Massively multiplex chemical transcriptomics at single-cell resolution. Science. 2020 Jan 3;367(6473):45–51.
8. Dini A, Barker H, Piki E, Sharma S, Raivola J, Murumägi A, Ungureanu D. A multiplex single-cell RNA-Seq pharmacotranscriptomics pipeline for drug discovery. Nature Chemical Biology. 2025 Mar;21(3):432–42.
9. Jiang L, Schlesinger F, Davis CA, Zhang Y, Li R, Salit M, Gingeras TR, Oliver B. Synthetic spike-in standards for RNA-seq experiments. Genome Research. 2011 Sep;21(9):1543–51.
10. Love MI, Huber W, Anders S. Moderated estimation of fold change and dispersion for RNA-seq data with DESeq2. Genome Biology. 2014 Dec 5;15(12):550.
11. Landais Y, Vallot C. Multi-modal quantification of pathway activity with MAYA. Nature Communications. 2023 Mar 25;14(1):1668.
12. Haupt Y, Maya R, Kazaz A, Oren M. Mdm2 promotes the rapid degradation of p53. Nature. 1997 May 15;387(6630):296–9.
13. Kubbutat MH, Jones SN, Vousden KH. Regulation of p53 stability by Mdm2. Nature. 1997 May 15;387(6630):299–303.
14. Errington F, Willmore E, Leontiou C, Tilby MJ, Austin CA. Differences in the longevity of topo IIα and topo IIβ drug-stabilized cleavable complexes and the relationship to drug sensitivity. Cancer Chemotherapy and Pharmacology. 2004 Feb;53(2):155–62.
15. Yang WS, SriRamaratnam R, Welsch ME, Shimada K, Skouta R, Viswanathan VS, Cheah JH, Clemons PA, Shamji AF, Clish CB, Brown LM. Regulation of ferroptotic cancer cell death by GPX4. Cell. 2014 Jan 16;156(1):317–31.
16. Koppula P, Zhang Y, Zhuang L, Gan B. Amino acid transporter SLC7A11/xCT at the crossroads of regulating redox homeostasis and nutrient dependency of cancer. Cancer Communications. 2018 Dec;38(1):1–3.
17. O'Brien J, Mitchell C, Auerbach S, Doonan L, Ewald J, Everett L, Faranda A, Johnson K, Reardon A, Rooney J, Shao K. Bioinformatic workflows for deriving transcriptomic points of departure: current status, data gaps, and research priorities. Toxicological Sciences. 2025 Feb;203(2):147–59.
18. Stuart T, Butler A, Hoffman P, Hafemeister C, Papalexi E, Mauck WM, Hao Y, Stoeckius M, Smibert P, Satija R. Comprehensive integration of single-cell data. Cell. 2019 Jun 13;177(7):1888–902.